# Numerical Simulation Study of the Magnetic Flux Tube Expansion on the Divertor Plasma Parameters by the LINDA Code*)

Md. Shahinul ISLAM, Yousuke NAKASHIMA[1)], Seiji ISHIGURO, Kazuo HOSHINO[2)], Akiyoshi HATAYAMA[2)], Hiroki HASEGAWA and Mizuki SAKAMOTO

*National Institute for Fusion Science, Toki, Gifu 509-5292, Japan*
[1)]*Plasma Research Center, University of Tsukuba, Tsukuba, Ibaraki 305-8577, Japan*
[2)]*Graduate School of Science and Technology, Keio University, Hiyoshi, Yokohama 223-8522, Japan*

(Received 22 October 2020 / Accepted 16 February 2021)

In this research, we investigate the effect of magnetic flux tube expansion on the divertor plasma parameters by using the fluid code "LINDA". A comparison between the cylindrical flux tube (without the magnetic flux expansion) and the expansion magnetic flux tube has been undertaken. The aim of the study is to understand the impact of magnetic field expansion on the divertor physics by using the LINDA fluid code. The plasma density ($n_\mathrm{i}$) is decreased and parallel velocity is increased ($u_{\mathrm{i}\|}$) toward the target plate with the expansion of magnetic field lines near the target plate. The heat and particle fluxes are reduced significantly on the target plate in the case of the expansion mesh configuration. For the case of cylindrical mesh, advection becomes stronger with the decreasing distance from the target plate. In the case of expansion mesh, diffusion is stronger with the decreasing distance from the target plate. These outcomes clearly indicate the effect of the magnetic field structure on the divertor plasma parameters.



Keywords: fluid simulation, LINDA code, plasma detachment, magnetic flux expansion, heat flux, ion flux

DOI: 10.1585/pfr.16.2403049

## 1. Introduction

In the magnetic confinement fusion reactors high temperature and density plasmas are to be confined in the core region. The impurities generate because the plasma-wall interactions can go in the vicinity of the core region. This process badly affects the fusion reactions in the core plasma region. Consequently, the divertor concept is developed to overcome the difficulties noted above. However, the suppression of the high heat load on the divertor target plates is an unsolved research issue to date. Therefore, it is necessary to reveal a scenario with the reasonable heat-flux on the target plates. The plasma detachment state is considered to be an efficient way to control the heat load on the target plate [1–5]. As a consequence, it is also necessary to understand fully the processes of plasma detachment in fusion devices.

The high heat load on the divertor target plate can be reduced via volume plasma recombination and by impurity radiation. Impurity particle reduces the plasma temperature in the divertor region, which makes a strong temperature gradient toward the core. As a result, the impurities are transported into the core region via thermal force. Impurity radiation is good for divertor region, but it can make thermal collapse in the core region. Thus, we need to think of a divertor regime with a reasonably lower impurity concentration. The heat load on the target plate can also be reduced by expanding the magnetic flux tube near the divertor target plate. More specifically, it is important to investigate the effects of (1) the magnetic connection to length to divertor plate, and (2) the magnetic flux tubes broaden on the divertor plasma physics.

Numerical simulation is an enormous way for understanding the physics of plasma detachment. In the innovative research, we have investigated the effects of magnetic flux tube on the divertor plasma parameters by using the multi-fluid code "LINDA" [6–11]. In the LINDA code, 2-D numerical mesh are formed in the cylindrical coordinate under the assumptions of axisymmetric. The LINDA is developed based on the B2 fluid code [12]. A tungsten (W) target plate is created at the end of the mesh, where divertor boundary conditions are imposed.

In this research, we investigate the effect of magnetic flux tube expansion on the divertor plasma parameters numerically by the LINDA code. More specially, two different magnetic field lines (expansion mesh and cylindrical mesh) are generated for investigating the effect of magnetic flux geometry on the divertor plasma. As a consequence, a comparison between the cylindrical flux tube (without the magnetic flux expansion) and the expansion magnetic flux tube has been undertaken in this innovative research work.

*author's e-mail: islam.mdshahinul@nifs.ac.jp, shahinulislamrony@gmail.com*

*) This article is based on the presentation at the 29th International Toki Conference on Plasma and Fusion Research (ITC29).

# 2. Numerical Simulation Model

## 2.1 Mesh structure

The simulation model for the cylindrical and expansion mesh structure is shown in Fig. 1. The LINDA code is a 2D code, which has been developed based on the axisymmetric condition. The number of mesh in the axial and radial direction are 66 and 50, respectively. The numerical mesh along with the axial directions are the same for both of the configurations ($z$ = 0 - 0.7 m). As for the expansion mesh case, the magnetic flux tube is expanded in the radial direction toward the target plate ($r$ = 0 - 0.15 m), as shown in Fig. 1 (a). On the other hand, for the cylindrical mesh case, the magnetic flux tube is uniform along the radial direction ($r$ = 0 - 0.15 m) in the entire mesh, as shown in Fig. 1 (b). As shown in Fig. 1, a target plate is located at the end of the mesh. The divertor boundary is applied on the target plate. More detailed descriptions of the LINDA code are given in the references [6–11].

## 2.2 Plasma fluid equations

The LINDA code consists of continuity equation (outputs plasma density, assume $n_\mathrm{i} = n_\mathrm{e}$), momentum balance equation (outputs parallel velocity), ion and electron energy equations (output are ion, and electron temperature). The hypotheses of the LINDA code are: (1) plasma is quasi-neutral and am-bipolar flow, (2) ion velocity is neglected in the diamagnetic direction, (3) anomalous and classical transport in the radial and perpendicular direction, respectively, (4) viscosity tensor is simplified, (5) effect of drift and of current is ignored, (6) electron mass has been considered as 0 (zero), consequently, the momentum balance equation has been numerically solved only for the ion, and (7) continuity equation is also solved only for ion, and electron density is assumed to be equal to ion density.

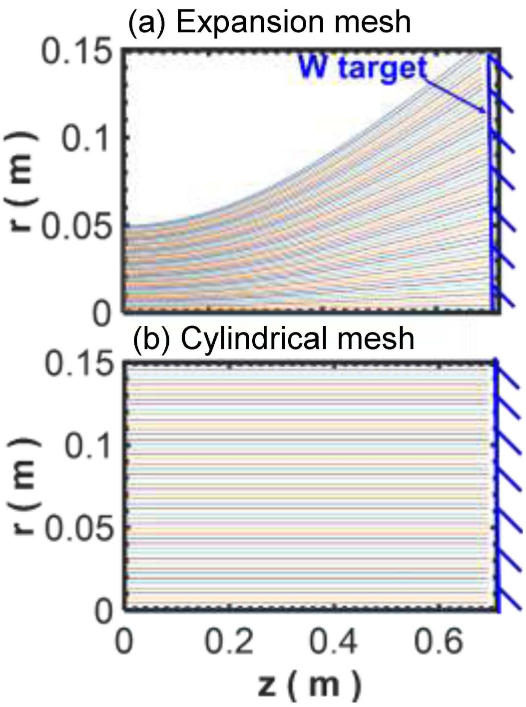


Fig. 1 Mesh structure of the simulation model (a) expansion mesh and (b) cylindrical mesh.

The fluid equations are:

$$\frac{\partial n_\alpha}{\partial t} + \frac{1}{\sqrt{g}}\frac{\partial}{\partial x}\left(\frac{\sqrt{g}}{h_x}n_i u_i\right)\frac{1}{\sqrt{g}}\frac{\partial}{\partial y}\left(\frac{\sqrt{g}}{h_x}n_i v_i\right) = S^i_n. \tag{1}$$

Momentum balance equation of ion species $\alpha$ is:

$$\begin{aligned}&\frac{\partial}{\partial t}(m_i n_i u_{\|i})\\ &\quad+\frac{1}{\sqrt{\sqrt{g}}}\frac{\partial}{\partial x}\left(\frac{\sqrt{g}}{h_x}m_i n_i u_i u_{\|i} - \eta^i_x\frac{\sqrt{g}}{h_x^2}\frac{\partial u_{\|i}}{\partial x}\right)\\ &\quad+\frac{1}{\sqrt{g}}\frac{\partial}{\partial y}\left(\frac{\sqrt{g}}{h_y}m_i n_i v_i u_{\|i} - \eta^\alpha_y\frac{\sqrt{g}}{h_y^2}\frac{\partial u_{\|i}}{\partial y}\right)\\ &= \frac{1}{h_x}\frac{B_\theta}{B}\left[-\frac{\partial p_i}{\partial x} - \frac{\partial p_e}{\partial x}\right] + S^i_{mu\|}.\end{aligned} \tag{2}$$

Diffusion approximation in the radial direction is:

$$v_\alpha = -\frac{1}{h_y}D^\alpha_n\frac{\partial}{\partial y}(\ln n_\alpha). \tag{3}$$

The ion energy balance equation:

$$\begin{aligned}&\frac{\partial}{\partial t}\left(\frac{3}{2}n_i T_i + \sum_\alpha \frac{1}{2}\rho_i u^2_{\|i}\right)\\ &\quad+\frac{1}{\sqrt{g}}\frac{\partial}{\partial x}\left[\frac{\sqrt{g}}{h_x}\left(\frac{5}{2}n_i u_i T_i + \frac{1}{2}m_i n_i u_i u^2_{\|i}\right)\right.\\ &\qquad\left.-\frac{\sqrt{g}}{h_x^2}\left(\kappa^i_x\frac{\partial T_i}{\partial x} + \frac{1}{2}\eta^i_x\frac{\partial u^2_{\|i}}{\partial x}\right)\right]\\ &\quad+\frac{1}{\sqrt{g}}\frac{\partial}{\partial y}\left[\frac{\sqrt{g}}{h_y}\left(\frac{5}{2}n_i u_i T_i + \frac{1}{2}m_i n_i v_i u^2_{\|i}\right)\right.\\ &\qquad\left.-\frac{\sqrt{g}}{h_y^2}\left(\kappa^i_y\frac{\partial T_i}{\partial y} + \frac{1}{2}\eta^i_y\frac{\partial u^2_{\|i}}{\partial y}\right)\right]\\ &= -\frac{u_e}{h_x}\frac{\partial p_e}{\partial y} - \frac{v_e}{h_y}\frac{\partial p_e}{\partial y} - k(T_i - T_e) + S^i_E.\end{aligned} \tag{4}$$

The electron energy balance equation:

$$\begin{aligned}&\frac{\partial}{\partial t}\left(\frac{3}{2}n_e T_e\right) + \frac{1}{\sqrt{g}}\frac{\partial}{\partial x}\left(\frac{\sqrt{g}}{h_x}\frac{5}{2}n_e u_e T_e - \kappa^e_x\frac{\sqrt{g}}{h_x^2}\frac{\partial T_e}{\partial x}\right)\\ &\quad+\frac{1}{\sqrt{g}}\frac{\partial}{\partial y}\left(\frac{\sqrt{g}}{h_y}\frac{5}{2}n_e v_e T_e - \kappa^e_y\frac{\sqrt{g}}{h_y^2}\frac{\partial T_e}{\partial y}\right)\\ &= \frac{u_e}{h_x}\frac{\partial p_e}{\partial x} + \frac{v_e}{h_y}\frac{\partial p_e}{\partial y} - k(T_e - T_i) + S^e_E.\end{aligned} \tag{5}$$

The $S^i_n$, $S^i_{mu\|}$, $S^e_E$, and $S^i_E$ express the loss (sink) and production (source) terms respectively for continuity, parallel momentum, electron, and ion energy equation during collisions of plasma and neutral particles. The ionization, charge-exhange and recombination rate of H are included in the present model [13].

The upstream boundary conditions are applied in front of the most left side of Fig. 1. The upstream boundary conditions are fixed during iterations. During the iteration process, the upstream boundary conditions are given below:

Electron heat flux,

$$F_e(z=0, r, N_{\mathrm{it}}) = \frac{5}{2} n_{\mathrm{e}} T_e u_i, \tag{6}$$

Ion heat flux,

$$F_i(z=0, r, N_{\mathrm{it}}) = \frac{5}{2} n_{\mathrm{i}} T_i u_i, \tag{7}$$

Particle flux,

$$\Gamma_i(z=0, r, N_{\mathrm{it}}) = n_{\mathrm{i}} u_i. \tag{8}$$

At the initial stage of iteration, the initial conditions of the plasma parameters are given based on the following four equations:

$$n_i(z, r, N_{\mathrm{it}}=1) = 1\times 10^{19} \times e^{-\frac{1}{2}\left\{\frac{r}{r_{0n}(z)}\right\}^2}, \tag{9}$$

$$T_i(z, r, N_{\mathrm{it}}=1) = 30 \times e^{-\frac{1}{2}\left\{\frac{r}{r_{0i}(z)}\right\}^2}, \tag{10}$$

$$T_e(z, r, N_{\mathrm{it}}=1) = 30 \times e^{-\frac{1}{2}\left\{\frac{r}{r_{0e}(z)}\right\}^2}. \tag{11}$$

$$u_i(z, r, N_{\mathrm{it}}=1) = \frac{1}{2}\sqrt{\frac{n_e T_e + n_i T_i}{m_i n_i}}. \tag{12}$$

Where, $r_{0n}$, $r_{0i}$, $r_{0e}$ indicate half maximum full-width of physical quantities, $r$ is spatial position of physical quantities in the radial direction, $N_{\mathrm{it}}$ is the number of iteration. The values of the half maximum full-width are given based on the typical experimental parameters of GAMMA 10/PDX.

The divertor boundary condition on the target plate are written below:

$$u_{i\parallel} \geq \sqrt{\frac{T_{\mathrm{i}} + T_e}{m_i}}. \tag{13}$$

Ion heat transfer coefficient through the sheath entrance:

$$\alpha_i = 3.5. \tag{14}$$

Electron heat transfer coefficient through the sheath entrance:

$$\alpha_e = 4.0. \tag{15}$$

The boundary conditions for the electron ($q_{\mathrm{e}}$) and ion ($q_{\mathrm{i}}$) energy balance equations on the target plate are as follows:

$$q_i = \alpha_i n_i u_{i\parallel} T_i, \quad q_{\mathrm{e}} = \alpha_e n_e u_{e\parallel} T_e. \tag{16}$$

The heat flux and particle flux on the target plate are:

Heat flux,

$$\mathrm{q} = q_i + q_e. \tag{17}$$

Particle flux,

$$\Gamma_i = n_i u_{i\parallel}. \tag{18}$$

Radial transport coefficients:

$$\kappa_{\perp\mathrm{i}} = 0.2 \times n_{\mathrm{i}},\ \kappa_{\perp\mathrm{e}} = 4.0 \times n_{\mathrm{e}},$$

and

$$\eta_{\perp} = 0.2 \times m_i \times n_{\mathrm{i}}.$$

## 3. Simulation Results and Discussion

The 2D profiles of plasma density and parallel velocity are shown in Fig. 2. As shown in the figure, the plasma parameters are strongly affected by the magnetic flux structure near the target plate. Compared to Figs. 2 (a) and (b), it is shown that the plasma density is decreased towards the target plate for the expansion mesh. In particular, the plasma density is shown to be 10 times higher for the cylindrical mesh compared to the expansion mesh, as shown in Figs. 2 (a) and (b). Furthermore, the radial plasma density gradient is lower for the expansion mesh compared to the

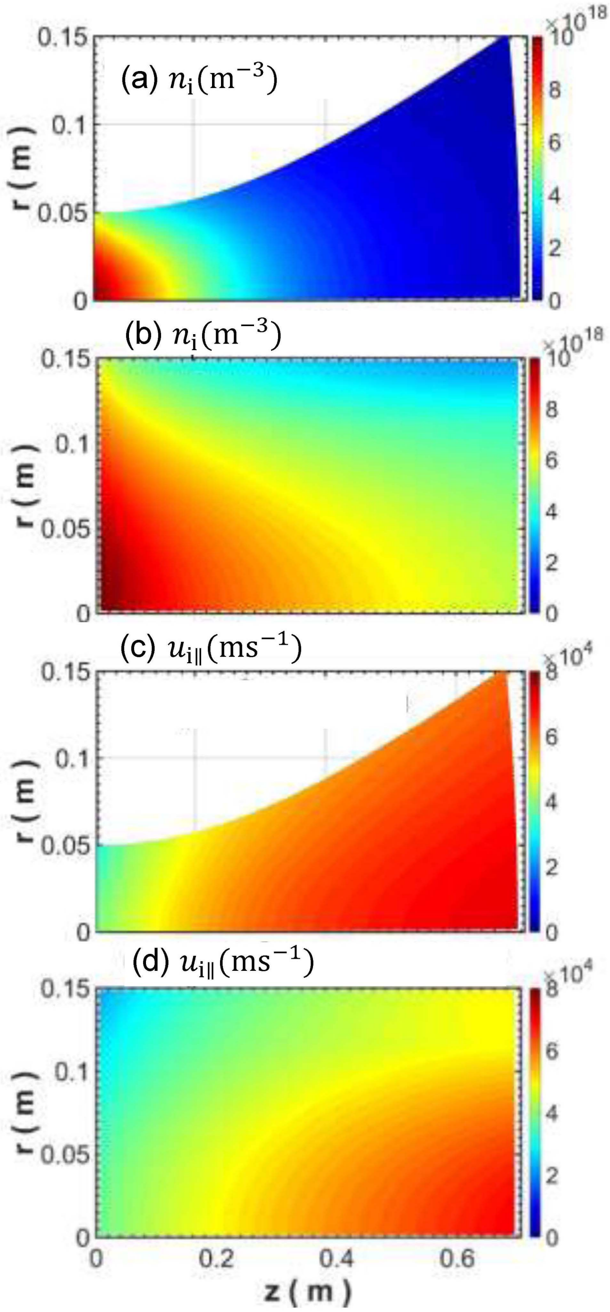


Fig. 2 2D profiles of plasma density for (a) expansion mesh, (b) cylindrical mesh, and 2D profiles of parallel velocity for (c) expansion mesh, (d) cylindrical mesh.

cylindrical mesh, as shown in Figs. 2 (a) - (b). As plasma density is decreased the heat conduction is also changed.

The ion parallel velocity is also strongly influenced by the magnetic flux expansion. The ion parallel velocity is increased near the target plate for the expansion mesh compared to cylindrical mesh, as shown in Figs. 2 (c) and (d). In order to understand the 2D results more clearly, the 1D profile of the plasma parameters are shown in Fig. 3.

The 2D profiles of ion and electron temperature are shown in Fig. 3. As shown in the figure, the ion temperature is affected by the magnetic flux structure near the target plate. Compared to Figs. 3 (a) and (b), it is shown that the ion temperature is decreased towards the target plate for the cylindrical mesh. Since the plasma density is higher for the cylindrical mesh (Figs. 2 (a) and (b)), the ion temperature is reduced via the electron-ion relaxation processes. On the other hand, the electron temperature is increased near the target plate for the cylindrical mesh compared to the expansion mesh, as shown in Figs. 3 (c) - (d).

The 1D profile of electron temperature ($T_e$) is shown

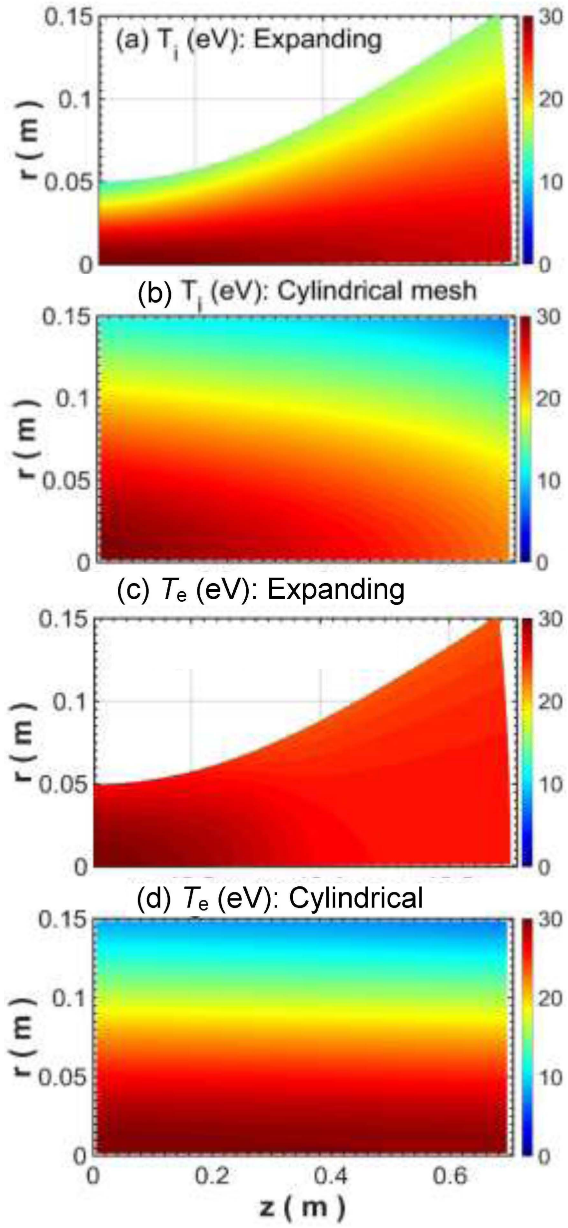


Fig. 3 2D profiles of ion temperature for (a) expansion mesh, (b) cylindrical mesh, and electron temperature for (c) expansion mesh, (d) cylindrical mesh.

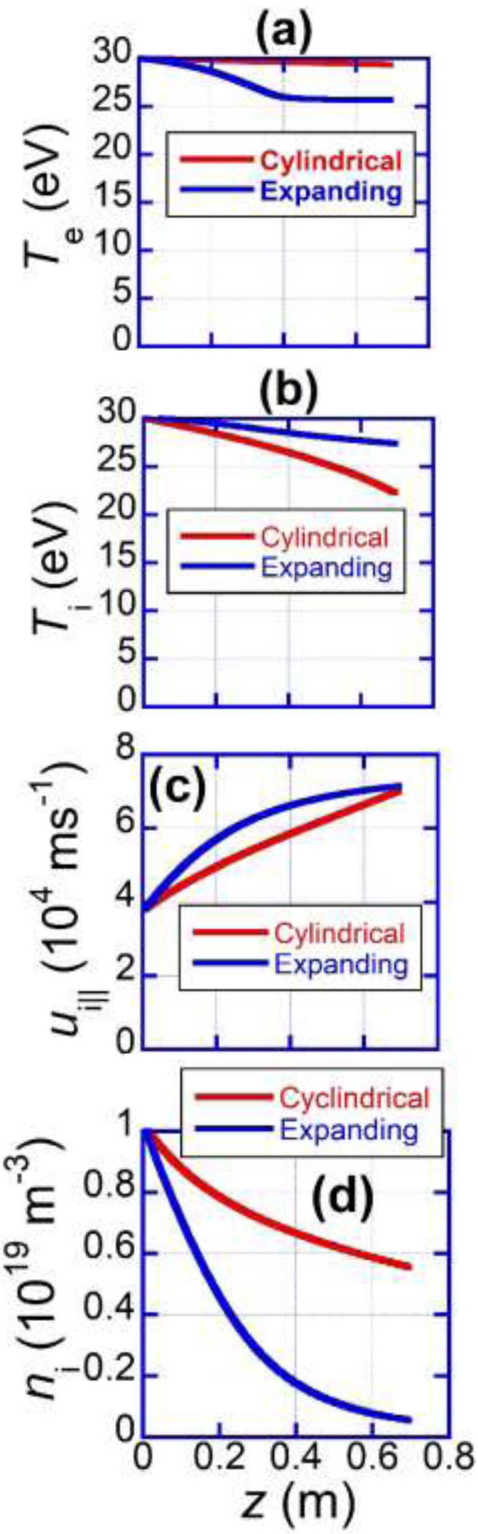


Fig. 4 Axial profiles of plasma parameters (at $r = 0$ m) (a) $T_e$, (b) $T_e$, (c) $u_{i\|}$, and (d) $n_i$.

in Fig. 4 (a). Since the plasma density is higher for the cylindrical mesh, the electron-ion collisions are enhanced. Consequently, the $T_e$ is shown to be higher for the cylindrical mesh than that of the expansion mesh, as shown in Fig. 4 (a). The 1D profile of ion temperature ($T_i$) is also shown in Fig. 4 (b). The ion temperature is shown to be lower for the cylindrical mesh compared to the expansion mesh, as shown in Fig. 4 (b). The electron-ion collisions affect the electron and ion temperature due to the difference in the plasma density for the cylindrical and expansion mesh.

The parallel velocity is shown to be lower for the cylindrical mesh compared to the expansion mesh, as shown in Fig. 4 (c). A consequence of the flux tube expansion is the difference of the parallel velocity around $z \sim 0.2$ - $0.5$ m in Fig. 4 (c). On the other hand, the parallel velocity on the target plate is shown to be similar for both the mesh structures, as shown in Fig. 4 (c). The Bohm boundary condition is applied on the target plate for the parallel velocity. As a consequence, the velocity on the target plate is determined by the divertor boundary condition.

The plasma density is shown to be significantly lower for the expansion mesh in comparison to the cylindrical mesh, as shown in Fig. 4 (d). Since the mesh area is expanded radially, the flow velocity is enhanced but the plasma density is reduced to maintain the particle balance of the continuity equation. As the plasma density is reduced, the heat conduction is also affected significantly.

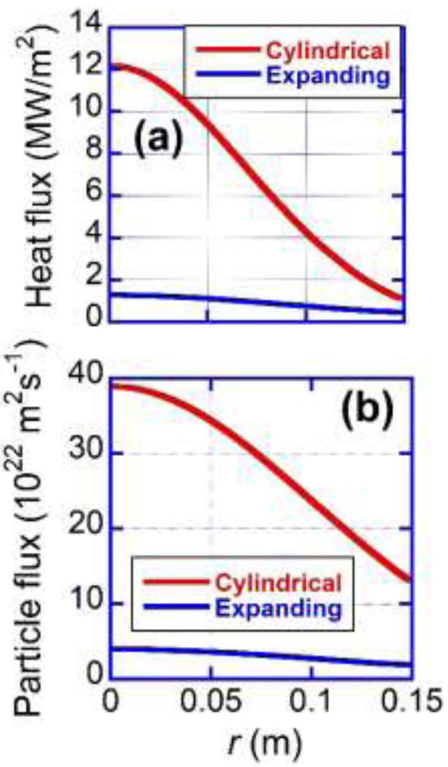


Fig. 5 Radial profiles of (a) heat flux and (b) particle fluxes on the target for the expansion and cylindrical mesh.

In this paper, the effects of magnetic flux expansion are investigated on the heat and particle fluxes on the target plate. The radial profile of the heat flux and particle flux on the target plate is shown in Fig. 5. The definition of the heat flux and the particle flux on the target plate are given in the equations 17 and 18, respectively. It is shown that the heat flux on the target plate is reduced remarkably in the case of expansion mesh compared to the cylindrical mesh, as shown in Fig. 5 (a). Moreover, the heat flux on the target plate is reduced by 10 times by expanding the magnetic flux tube, as shown in Fig. 5 (a). The particle flux on the target plate is shown to be 10 times lower in the case of expansion mesh than that of the cylindrical mesh, as shown in Fig. 5 (b).

More detailed investigation is necessary for understanding the impact of magnetic field structure on the divertor physics. The physical mechanism will be investigated in the future.

## 4. Summary

The effects of magnetic field structures on the plasma parameters toward the target plate have been investigated numerically by using the LINDA code. Plasma density decreases with the expansion of the magnetic field. Interactions between ion and electron increase under the condition of cylindrical mesh. The heat flux and particle flux are found to be 10 times lower in the case of expansion mesh compared to the cylindrical mesh. It seems that decrease of particle and heat fluxes depends on the cross-section area of magnetic field. It is possible to generate large energy loss area in plasma by expanding magnetic field lines toward the target plate.

## Acknowledgments

This study was supported by the bidirectional collaboration research program of the University of Tsukuba, and National Institute for Fusion Science (NIFS19KUGM140).

[1] P.C. Stangeby, Plasma Phys. Control. Fusion **43**, 223 (2000).
[2] A. Loarte *et al.*, Nucl. Fusion **47**, S203 (2007).
[3] A. Kallenbach *et al.*, Plasma Phys. Control. Fusion **58**, 045013 (2016).
[4] S. Takamura *et al.*, J. Plasma Fusion Res. **4**, 138 (2001).
[5] N. Ohno, Plasma Phys. Control. Fusion **59**, 034007 (2017).
[6] M.S. Islam *et al.*, Nucl. Mater. Energy **18**, 182 (2019).
[7] M.S. Islam *et al.*, Fusion Eng. Des. **125**, 216 (2017).
[8] M.S. Islam *et al.*, Plasma Phys. Control. Fusion **61**, 125005 (2019).
[9] M.S. Islam *et al.*, Plasma Fusion Res. **13**, 3403080 (2018).
[10] M.S. Islam *et al.*, Contrib. Plasma Phys. **58**, 805 (2018).
[11] M.S. Islam *et al.*, Plasma Phys. Control. Fusion **59**, 125010 (2017).
[12] B.J. Braams, NET Rep. 68 EURFU/X-80/87/68, CEC, Brussels (1987).
[13] D.E. Post *et al.*, J. Nucl. Mater. **220**, 143 (1995).